Autonomous Inspection and Data Fusion for Maritime Critical Infrastructures

1st Fletcher Thompson
National Institute for Aquatic Resources
Technical University of Denmark
Kongens Lyngby, Denmark
fletho@aqua.dtu.dk

2nd Peter Nicholas Hansen
Dept. of Electrical and Photonics Engineering
Technical University of Denmark
Kongens Lyngby, Denmark
pnha@dtu.dk

3rd Roberto Galeazzi
Dept. of Electrical and Photonics Engineering
Technical University of Denmark
Kongens Lyngby, Denmark
roga@dtu.dk

4th Marco Palma
UBICA s.r.l., Underwater BIo CArtography
Genoa, Italy
info@ubicasrl.com

5th Andreas Libonati Brock
Copenhagen Municipality
Copenhagen, Denmark
WD0Y@kk.dk

6th Patrizio Mariani
National Institute for Aquatic Resources
Technical University of Denmark
Kongens Lyngby, Denmark
pat@aqua.dtu.dk

***Abstract*—Automation and robotics are essential for the effective monitoring and inspection of maritime critical infrastructures and marine environments. We demonstrate the use of an unmanned surface vehicle, integrated with acoustic and optical sensors, to perform fast and accurate inspections of maritime infrastructures in confined areas (i.e., presence of buildings and multiple obstacles). High resolution maps are obtained fusing offline data from LiDAR and 2D acoustic multi-beam forward looking camera point clouds. The technological pipeline is demonstrated through a survey in Copenhagen harbour. The data acquisition leverages on methods to improve path planning and localization to correct failures in the RTK GNSS due to shadowing of buildings and other obstacles. The entire data flow is streamlined to produce fast delivery time and data access, optimizing data acquisition and processing, providing results into a dedicated web service tailored to users' needs for knowledge and information extraction.**

***Index Terms*—Sensor Fusion, Surveillance, infrastructure monitoring, forward looking sonar, LiDAR**

I. Introduction

The effective monitoring of maritime infrastructures is a major requirement to support the development of a sustainable ocean economy as ports, undersea cables, offshore installations are all vital components of the global economy supporting social security [1]. As a consequence, the requests to perform cost effective maintenance and inspection tasks have increased across different sectors including offshore oil and gas, transport and renewable energy industry [2]. At the same time similar demands for cost effective mapping solutions are present across different environmental agencies to monitor marine biodiversity, pollution and ecological conditions since the increases in some maritime activities have implications for healthy marine ecosystems [3]–[5]. In recent years, threats to critical marine infrastructure have also impressed the urgency and importance of regular and detailed mapping for anomalous threat detection [6] above and below the water surface. Underwater threat detection is a challenging task, requiring both accuracy and scalability of mapping solutions. This task is compounded in scenarios where Global Navigation Satellite System (GNSS) quality is poor or denied due to occlusion from physical structures (bridges and tall buildings), or adversarial attacks on GNSS infrastructure. Solutions to GNSS denied underwater mapping exist in the state-of-the-art, typically using high-resolution 3D multi-beam echosounder coupled with a high-accuracy inertial navigation system [7]. However the scalability of these systems is limited due to the significant costs associated with the hardware. Low-cost underwater mapping can be achieved with cheaper Foward Looking Sonar (FLS), and reconstructing accurate 3D data from FLS is an active field of research [8]–[10]. In this work, we present a new method for extracting 3D data from FLS by exploiting the orientation of the FLS with respect to a structured scene (in this case, harbor walls and seabed). Even with such 3D data, positioning in partially or completely GNSS

Research co-financed by City of Copenhagen, The Technical and Environmental Administration.
This article is delivered under the partial support of the EU H2020 MISSION ATLANTIC project under the EU Research and Innovation Program grant agreement No. 639 862428.
This work is also partially supported by the project OCEAN CITIZEN which is Co-funded by the European Union, under Horizon Europe Research and Innovation programme, No. 101093910.

denied environments is better achieved by above-waterline Simultaneous Localisation And Mapping (SLAM) algorithms applied to camera, Inertial Measurement Unit (IMU) and Light Detection and Ranging (LiDAR) sensor data since noise, multi-pathing effects, and active ranging beam widths are much less in-air. In the context of this work, we propose a low-cost, fast, accurate, and scalable approach for mapping of underwater infrastructure in partially or completely GNSS denied environments by combining LiDAR, IMU and FLS using our own algorithm for FLS 3D target positioning. The payloads are configured on an Uncrewed Surface Vehicle (USV), which was deployed in Copenhagen harbour for a field trial. The results show that relatively inexpensive equipment can be used in structured marine environments to rapidly produce high resolution 3D maps, indicating that such systems could be scaled effectively for persistent wide-spread infrastructure monitoring.

II. Methods

A. Platform definitions

The autonomous inspection system consists of the following components:

1) The Maritime Robotics™ USV *Otter* with Real-time Kinematic (RTK) GNSS.
2) A Teledyne BlueView™ m900/2250 mkII FLS.
3) An Ouster™ OS1 LiDAR coupled with a 6-axis IMU.

The USV is lightweight (50 - 70 kg) and requires low-effort logistics for transport, launch and recovery. The catamaran configuration and arrangement allows for modular payloads to be integrated in the aft section of the platform. In our case we have integrated the LiDAR and FLS as separate, modular payloads (see Figure 5). The USV communicates with shore-based operators over long range Wi-Fi and is represented as a simplified distributed system in Figure 1. Operators have online access to the configuration of the sensors and the platform. The sensor drivers are accessed by Robot Operating System 2 (ROS2) nodes, and logging of the sensor data and platform navigation data are also managed by ROS2. The Otter Raspberry Pi serves as a lower-stratum Network Time Protocol (NTP) server for synchronization of the sensor payload Pis, and it synchronizes with either internet-based NTP servers if 4G reception is available, with RTK GNSS updates, or using its own hardware clock.

B. FLS 3D Scanlines

Typically, an FLS has its receiving transducer array located on a 2D plane (most commonly in a line) that is parallel to the main lobe axis of the sending transducer. Figure 2 shows the coordinate system of the FLS' receiving main lobe (beamformed) axis (aligned with the red x axis), which has a horizontal and vertical aperture of $\Psi = 130°$ and $\Theta = 20°$ respectively. The positions of targets within the backscatter are represented in spherical coordinates relative to this coordinate system by range (r), azimuth (ψ) and elevation (θ). The planar arrangement of transducers introduces ambiguity in the elevation of the backscatter since it acts as a plane of symmetry

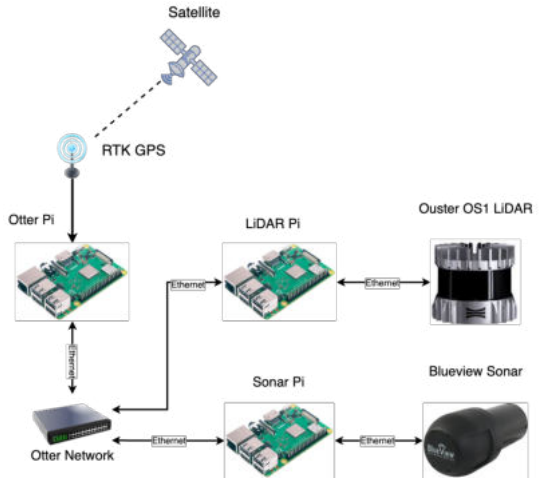

Fig. 1. Overview of the platform computer and payload setup.

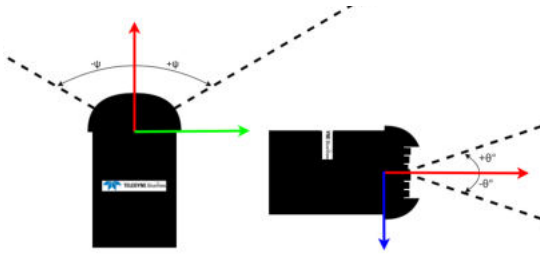

Fig. 2. The coordinate system of the FLS with x, y and z axes shown in red, green respectively. The transducer array can accurately resolve targets in range and azimuth (ψ), but is ambiguous in the elevation (θ).

(i.e. targets that are above the plane could also produce the same signal as mirror targets below the plane). Such sonar are used to produce 2D images and cannot be used for direct 3D reconstruction, but are much less expensive than multi-beam echosounder technology that solves this problem. However, since harbor inspections are typically a well-known structured environment, we can exploit information about the survey setup and operation to introduce a bias in the FLS backscatter signal that makes reconstructing the 3D position for a slice of the backscatter possible.

We take advantage of two facts of a typical harbour inspection survey (illustrated in Figure 3):

1) The USV moves more or less parallel to the inspection surface.
2) The FLS is oriented such that the main lobe centerline is between the the forward axis vector of the USV and the inspection surface normal.

Such a trajectory could be obtained with a closed-loop control strategy where observations of the wall are used to correct the heading of the USV to maintain a parallel relationship. In our case, we use open loop control from a human pilot to maintain this relationship.

This introduces a bias in the backscatter signal, since the closest observable backscatter signal is most likely to be on the outer edge of the main lobe of the receiving beam

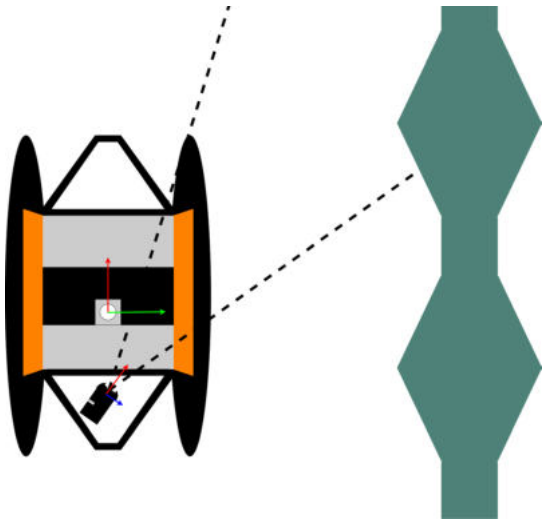

Fig. 3. Orientation of the survey allows exploitation of the nearest observable return signal to be mapped to a specific elevation. The shortest distance is biased towards the outer edge of the main lobe (in this example, $-\frac{\Theta}{2}$)

pattern closest to the inspection surface (assuming the surface does not have steep changes in normals). By implementing a thresholded rising edge detection algorithm (see Algorithm 1) along the range of each beam formed across ψ by the FLS' beamforming algorithm, we assign $\theta = -\frac{\Theta}{2}$ and extract the Cartesian coordinates.

Algorithm 1 Locate Nearest Target in Acoustic Imagery

Require: B (backscatter image in polar coordinates), T (minimum threshold for detection), M (minimum range for detection), Δ (resolution of range in units / sample), Ψ (Horizontal aperture width in rad), Θ (Vertical aperture width in rad)

Ensure: A Profile object containing the detections

$M_i \leftarrow \text{int}(M/\Delta)$
Initialize $occupancy$ array where $B \geq T$
Set $occupancy[:M_i]$ to False
$i \leftarrow \text{argmax}(occupancy, \text{axis=0})$ {Find nearest target}
$r \leftarrow i \times M$
$\psi \leftarrow \text{linspace}(-\Psi/2, \Psi/2, \text{length}(i))$
$\theta \leftarrow -\Theta/2$
$x \leftarrow r \cdot \sin(\psi) \cdot \cos(\theta)$
$y \leftarrow r \cdot \sin(\psi) \cdot \sin(\theta)$
$z \leftarrow r \cdot \cos(\theta)$
return x, y, z

Within the ROS2 ecosystem, the extracted scanlines for each ping are then converted to untextured point cloud data with the reference frame defined as `/sonar`. Transformations between the `/sonar` frame and the `/os_sensor` frame are measured and defined within ROS2 for registration into the LiDAR's generated `/map` frame as shown in the next section.

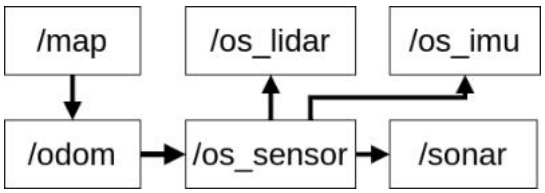

Fig. 4. Overview of the ROS2 transforms used for the LiDAR odometry and map generation, using RTAB-Map.

C. LiDAR

In order to facilitate autonomous inspection of critical maritime infrastructures, a complete map of the environment should be generated, which includes a 3D reconstruction of the above surface environment. This map can then be used both for visual verification of the environment for the human operator, and for localisation purposes for the autonomous system. The Ouster OS1 LiDAR is used for the generation of the map. The use of a LiDAR sensor also serves as an odometry source, which can be used to estimate the pose of the vehicle when the GNSS estimated positions are uncertain, i.e., when shadowing of large buildings are interfering with the signals.

The proposed method uses the open source library *RTAB-Map* [11], for the LiDAR based odometry and map generation. As RTAB-Map is a *loop closure* based SLAM approach, the mapping is independent of the odomentry approach, i.e., the chosen odometry method could be either visual, LiDAR or simply wheel based. RTAB-Map utilises an Iterative Closest Point (ICP) registration scheme to match the individual point clouds generated by the LiDAR, which is used to determine the odometry of the system from the LiDAR points. In the proposed pipeline, the RTAB-Map implementation provided in the ROS2 package `RTAB-Map`[1] is used. The following topics from the `RTAB-Map` package are used:

- `/cloud_map`: the assembled map (in `/map` frame).
- `/mapPath`: the estimated LiDAR odometry path (in `/odom` frame).

Figure 4 shows the different transforms defined for the LiDAR odometry and how they are related. At initialisation of the algorithm, the transforms from `/map` to `/odom` frame and from `/odom` to `/os_sensor` frame, are set to zero translation and rotation, i.e., the frames are equal to each other. When running the RTAB-Map algorithm, a successful ICP registration will result in an update to `/odom`

III. Results

A. Field Trial

As part of a pilot water quality monitoring and mapping project supported by the Copenhagen municipality, the USV and sensor payloads were deployed (Figure 5) in Belvedere's channel (55°39'16.3"N, 12°33'09.5"E). One objective of the survey was to scan the harbor walls and some of the bottom of the channel.

[1]https://github.com/introlab/rtabmap_ros

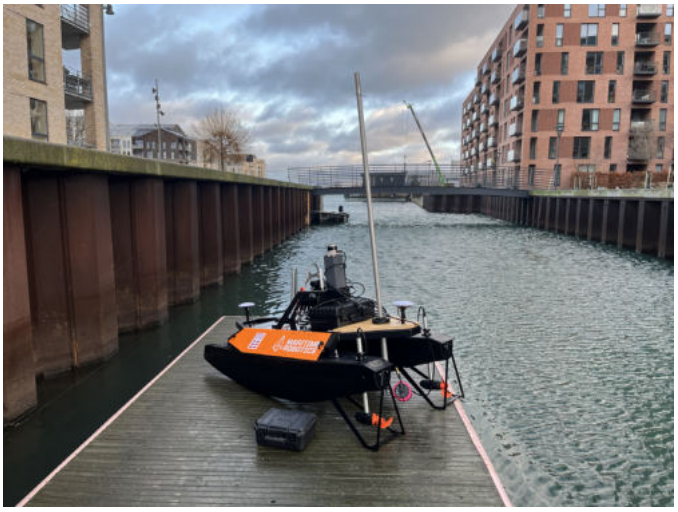

Fig. 5. Assembled USV just before deployment from a kayak ramp approximately 200 m from the survey site. FLS (see pink object) and LiDAR (device on rectangular mast) configurations are shown. Note the high walls of the channel, bridges, and tall buildings in the area.

Since the expected range to target was very short (i.e. $<$10 m), the FLS was configured to use the 2.25 MHz frequency for maximum range resolution (approximately 6 mm) and update at approximately 15 Hz. The FLS was rotated 90°, 45°, and then 15° with respect to the USV's body-fixed frame (following standard SNAME Forward-Starboard-Down convention) in extrinsic Euler angles, causing the sonar to point in a direction similar to Figure 3. The LiDAR was mounted on a mast for clearance, and configured to sample at 10 Hz with 1024 samples per rotation.

The complete system was rapidly deployed: it was transported in standard panel van, assembled at the launch site within 60 minutes, and was launched and recovered from points with 30 cm freeboard clearance using just two personnel. During the deployment, it was observed that the high channel walls, pedestrian bridges, and tall residential buildings in the survey area caused significant multi-pathing interference on the RTK GNSS. This prevented autonomous mode, and the USV was manually piloted through the channel using a mobile app over Wi-Fi. The pilot kept a constant distance of 2 m from the channel walls, and several rounds of the channel were conducted. Based on the effort expended within the survey area, the USV could cover approximately 3 - 5 km of infrastructure inspection transects within a 6 hour deployment window (depending on operator experience).

B. Point cloud views

In order to assess the accuracy of the generated SLAM map, the position of of five arbitrarily selected points was measured using an RTK GPS, where each point was measured twice, with at least 90 minutes between each measurement, to ensure different satellite constellations. Fig. 6 illustrates the geolocation of the five selected points overlayed on google earth, and the average UTM Northing and Easting coordinates

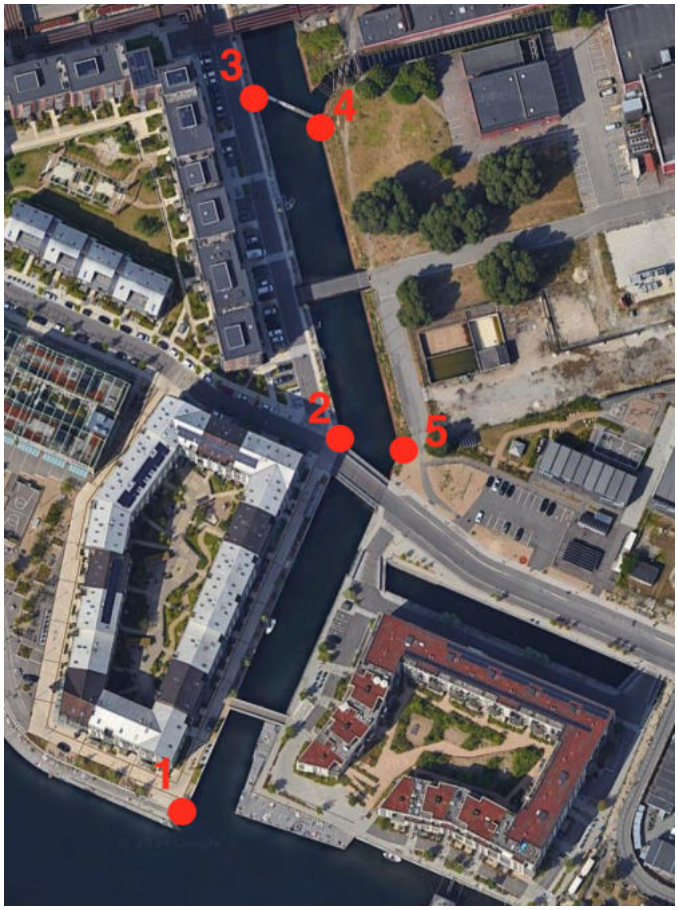

Fig. 6. RTK Measurement points overlayed on Google Earth image of Belvedere Channel.

TABLE I
THE MEASURED NORTHING AND EASTING COORDINATES OF THE POINTS ON THE MAP IN FIG. 6, AS MEASURED BY AN RTK GPS, AND THE x AND y VALUES OF THE SAME POINTS LOCATED IN THE GENERATED POINTCLOUD. COPENHAGEN IS IN UTM ZONE 32.

	RTK	
Point #	Northing (m)	Easting (m)
1	6173332.47	723473.96
2	6173463.65	723522.41
3	6173580.75	723486.57
4	6173569.99	723508.85
5	6173461.96	723541.97

are shown in Table I. From the five RTK points, four different line segments are constructed, such that

- Segment A: from point 1 to point 2,
- Segment B: from point 2 to point 3,
- Segment C: from point 3 to point 4,
- Segment D: from point 4 to point 5.

The length of each of the four segments are calculated from the L2-norm using the Northing and Easting coordinates of the RTK points in Table I. To obtain the lengths of the segments in the generated LiDAR pointcloud, the `lidarViewer` tool from MATLAB is used to directly measure the distances in

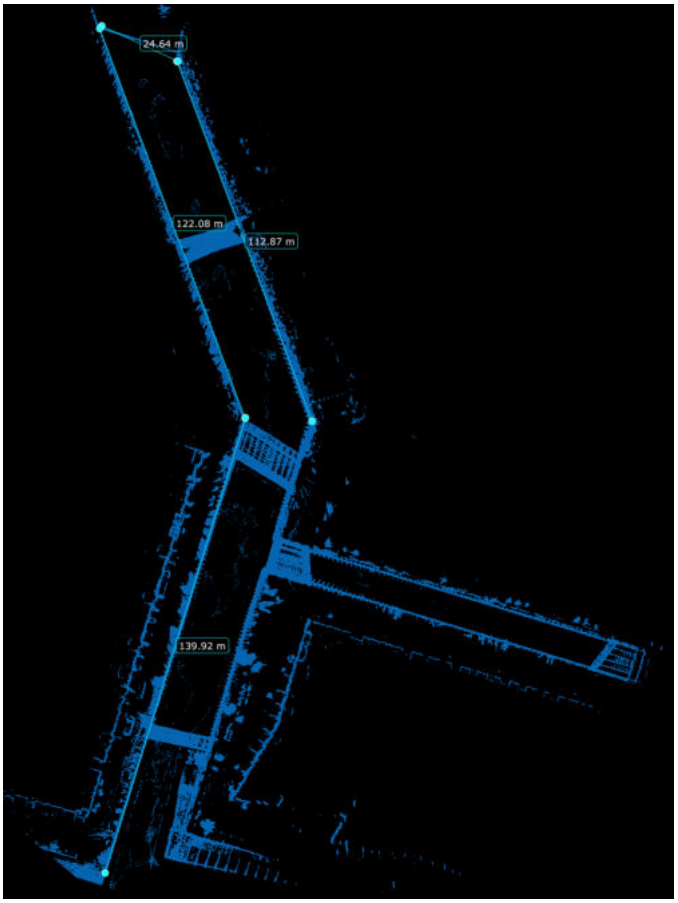

Fig. 7. The measured distances of the RTK points in the point cloud generated by RTAB-Map. Note, the distances shown are computed using MATLAB's builtin `lidarViewer` tool.

TABLE II
THE MEASURED LENGTHS OF THE LINE SEGMENTS FOR BOTH THE RTK GPS AND THE LIDAR POINTS. THE LIDAR DISTANCES ARE OBTAINED USING THE BUILTIN TOOLS PROVIDED IN THE MATLAB `LIDARVIEWER` TOOL.

	Segment Length		Error	
Segment	RTK (m)	LiDAR (m)	Absolute (m)	Relative (%)
A	139.84	139.92	0.08	0.05
B	122.46	122.08	0.38	0.31
C	24.74	24.64	0.10	0.42
D	112.99	112.87	0.12	0.11

the pointcloud, as illustrated in Fig. 7. The calculated RTK segment lenghts, and the measured LiDAR segment lengths, including the relative error, is shown in Table II. From Table II it is evident that the absolute error is approximately 0.1m for all but one of the line segment, which is 0.38m. However, the largest error is on a segment which is $\approx 122\text{m}$ long, which is also seen from the relative error, which is less than 0.5% for all of the line segments. It should be noted that the LiDAR segment lengths, depend on the selection of LiDAR points, which is a manual process, and is thereby naturally affected by selection of the correct/closest point in the pointcloud.

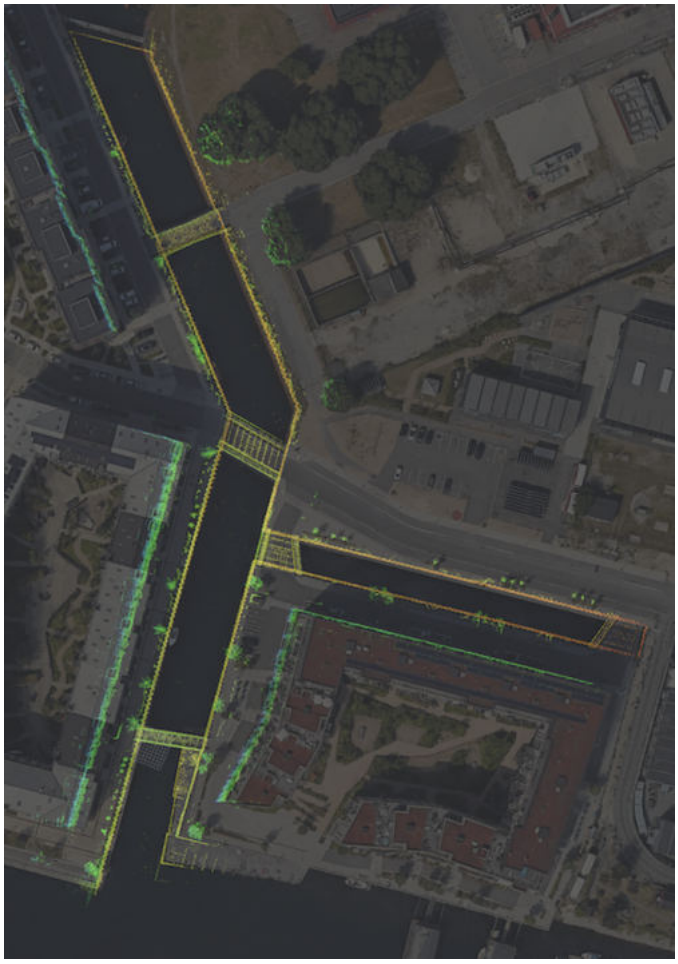

Fig. 8. LiDAR map overlayed on Google Earth image of Belvedere Channel.

The RTAB-Map assembled LiDAR pointcloud data, overlayed on Google Earth, is shown in Figure 8, where the geo-registration was performed with manual affine transformations (rotation and constant aspect-ratio scaling), visually affirming the the accuracy of the LiDAR/IMU SLAM generated map. However, the affine transformation could also be obtaining by the use of the RTK measurement points, and matching them to the respective points in the LiDAR pointcloud, however, for the specific task in Sydhavn this level of accuracy was not required.

The pose graph of the LiDAR produced by RTAB-Map was used to rotate and translate the FLS scanline data using the tf2 library in ROS2 [12]. Both pointcloud datasets were merged and are shown in figures 9 & 10.

In addition to geographic registration accuracy, the above surface and below surface point clouds need to be checked for consistency. From inspection of the data, the harbour "curtain" wall was identified as a consistent structure present in both above and below the waterline. We manually extract two point sets of the curtain wall, one above and one below the water line of 1 m in height and across approximately a 500 m² area. These sets are then compared by first projecting them onto a

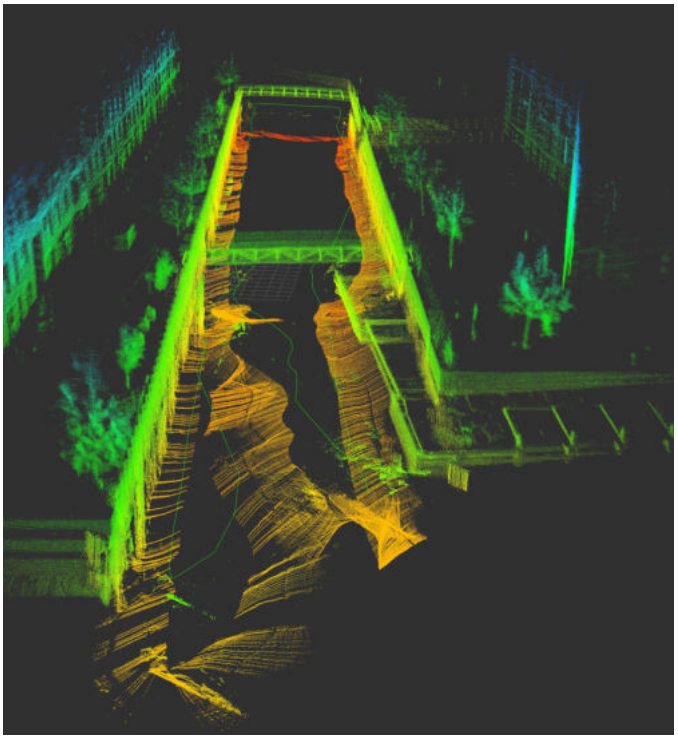

Fig. 9. Combined point cloud of LiDAR and FLS map overlayed on Google Earth. The coloring of the points reflect the z-value, i.e., height, mapped between $z \in [-8, 20](\mathrm{m})$.

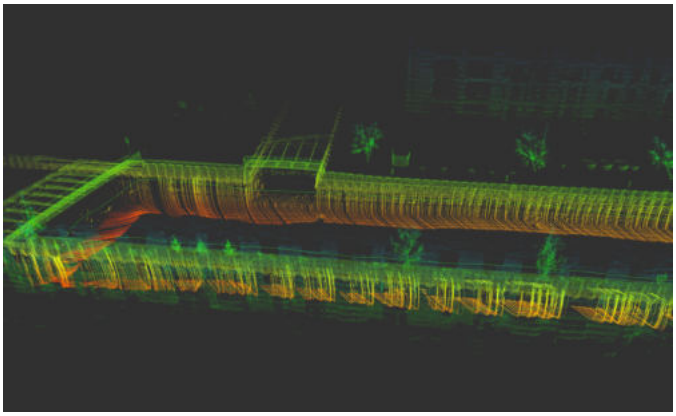

Fig. 10. Combined point cloud of LiDAR and FLS map overlayed on Google Earth. The coloring of the points reflect the z-value, i.e., height, mapped between $z \in [-8, 20](\mathrm{m})$.

common plane to eliminate the z component offsets, closeups of the result are shown in Figure 11.

We then fit a point registration transformation using ICP initialized with an identity matrix (since the two datasets are already aligned by our measured LiDAR - FLS offset and rotation). The quality of the registration is represented in the percentage of inliers used, the Root Mean Squared Error (RMSE) of the aligned point sets, and the cosine similarity of the computed transformation with I_4. In our studied area, 45% of the combined points were inliers, with an RMSE of 0.05 m

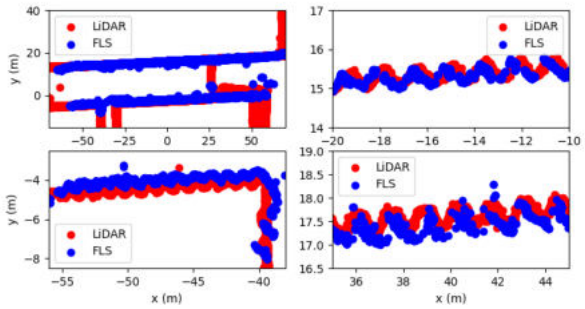

Fig. 11. Top left: the region used in the comparison. Top right: wall segments appear slightly out of phase. Bottom left: wall segments appear to be aligned but offset from each other. Bottom right: wall segments appear slightly out of phase.

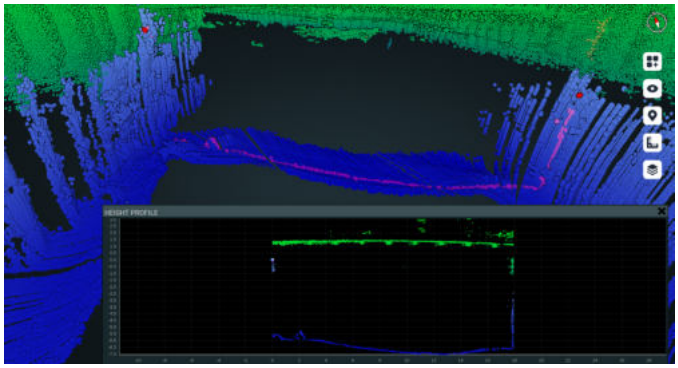

Fig. 12. Visualization of a profile slice of the Belvedere's channel pointcloud.

and transformation cosine similarity to I_4 of 99% indicating a consistent structure between the two datsets despite local inaccuracies (see Figure 11.

Viewing and analyzing large pointcloud datasets usually requires hardware accelerated compute resources, and specialized software such as MeshLab, CloudCompare or, in the case of figures 8-10 RViz. We host the produced pointcloud data results through Ubica S.R.L.[2], which allows viewing and analysis of pointclouds, such as obtaining sliced profile data, on web-browsers and on mobile devices (Figure 12).

IV. Discussion

Ports serve as critical hubs for studying interactions between drivers and pressures on the marine environment, offering opportunities to gain insight on coastal dynamics and marine ecosystems. These areas are key interfaces where terrestrial and marine environments converge, making them ideal sites for scientific investigation and technology development to support the sustainable management of: biodiversity, city run-off and pollution, ballast waters, shipping and recreational activities. Those activities are essential to promote informed spatial planning in marine urban context, as well as to develop new economic and living opportunities.

[2]https://oceancitizen.ubicasrl.com/viewer/Embankment2#

Here we demonstrate the use of a USV, that has been integrated with high resolution acoustic and optical sensors, to perform fast and accurate mapping and monitoring of the Copenhagen port within a densely populated urban environment. The presence of obstacles impaired RTK GNSS connection and affect the accuracy of the mapping. Our method for data acquisition demonstrates how sensor fusion can be used to correct failures in the localization due to shadowing of buildings and other obstacles. LiDAR, IMU and FLS measurements have been aligned and combined to obtain accurate positioning and to deliver high resolution maps of the area, both for the above and underwater structures. We notice that the failures in geolocalization can represent a more general challenge for conducting autonomous operations also in offshore installations, where presence of large metal structures can create similar obstructions to the the RTK GNSS signal.

The FLS scanline extraction method is an improvement over previous methods where the FLS is pointed perpendicularly to the inspection surface since the backscatter is biased to be closer to one side of the FLS' elevation. It is foreseeable that this method could be challenged by structures with abrupt changes in direction (such as in 90° corners or ledges) since the closest observed distance could be at an elevation angle that is not at the extremities of the main lobe. Additionally, shadows cast by ridges and objects peaking out of the main surface are more prominent due to the angled beam. Thus we recommend surveys to include transects in the opposite direction to completely resolve the shadowed areas. Close observations of the differences between the FLS and LiDAR datasets reveal distance offsets both along and perpendicular to the wall. While these differences are minor in the global alignment, they are most likely due to sensitivity of the FLS to the calibration of the vertical aperture of the FLS, sound velocity in the water column, accuracy of measured transformation between LiDAR and FLS coordinate frames, as well as LiDAR and IMU coordinate frames. All of these points can be addressed by calibration methods such as standard target acoustic calibration, sound velocity profiling, and calibrated target patch tests. For future works, parameter adjustment of the FLS data could be introduced by comparing LiDAR with corresponding FLS measurements on structures known to be consistent above and below the waterline.

In our application, the output pointcloud data has been further integrated into commercially available online visualization software developed by one of the co-authors in this manuscript[3]. The entire data flow is streamlined to produce fast delivery time and data access for timely and well-informed decision-making, which are generally required in port environments in cases like spillover of chemical substances, accidents and emergency scenarios.

The mapping and inspection technology presented here well aligns with the requirements implied by the development of the Digital Twin of the Ocean (DTO) [13]. The DTO is a digital representation of physical entities, environments, or systems, such as offshore oil rigs, wind farms, ports or even entire cities. By constantly syncing with its physical counterpart through sensors, data streams, and advanced analytics, it provides real-time insights into its status, performance, and potential issues. This enables end-users to remotely monitor, diagnose, and even simulate scenarios to improve decision-making and operational effectiveness.

The system presented here can be effectively incorporated into a DTO to support further applications based on e.g., artificial intelligence, machine learning, and predictive analytics, to, e.g., anticipate maintenance needs, forecast performance trends, and optimize resource utilization proactively. For instance, in the context of port and maritime infrastructures, the accurate and fast mapping can be used to predict infrastructure failures, optimize energy provision, and even simulate emergency scenarios for training purposes. Incorporating our data stream into a proper DTO cyberinfrastructure can enhance operational efficiency and cost-effectiveness in port environments and can contribute to the sustainability efforts of urban areas by minimizing dissipation of resources and by reducing environmental impacts of antropogenic activities.

[3]https://www.ubicasrl.com

V. Conclusions

We demonstrated how the utilization of advanced sensor-integrated USV enable fast and accurate mapping and monitoring within port environments, even amid densely populated urban settings like Copenhagen. Despite challenges posed by obstacles, our approach employing sensor fusion techniques ensures precise localization and comprehensive coverage of both surface and underwater structures. Furthermore, our refinement of FLS extraction methodologies enhances inspection processes, albeit with certain limitations in complex environments. Integration of point cloud data into online visualization platforms enables rapid decision-making and response during critical scenarios. This aligns seamlessly with the concept of DTO, offering real-time insights and predictive analytics for optimizing port operations. Looking forward, the technology and advancements presented here hold big promises in supporting sustainable urban development by minimizing resource dissipation and mitigating environmental impacts, thereby fostering a future where efficiency, resilience, and security needs will all converge.

Acknowledgment

FT and PM thank R. Garmund and H. Hansen from DTU Aqua's workshop for timely manufacture and quality assurance of the integrated FLS payload.

References

[1] A. Del Grosso, "Monitoring of infrastructures in the marine environment," in *Structural Control for Civil and Infrastructure Engineering*, 02 2001, pp. 107–117.

[2] D. O. Jones, A. R. Gates, V. A. Huvenne, A. B. Phillips, and B. J. Bett, "Autonomous marine environmental monitoring: Application in decommissioned oil fields," *Science of The Total Environment*, vol. 668, pp. 835–853, 2019. [Online]. Available: https://www.sciencedirect.com/science/article/pii/S0048969719308137

[3] N. Barrett, J. Seiler, T. Anderson, S. Williams, S. Nichol, and S. Nicole Hill, "Autonomous underwater vehicle (auv) for mapping marine biodiversity in coastal and shelf waters: Implications for marine management," in *OCEANS'10 IEEE SYDNEY*, 2010, pp. 1–6.

[4] H. Flores, N. H. Motlagh, A. Zuniga, M. Liyanage, M. Passananti, S. Tarkoma, M. Youssef, and P. Nurmi, "Toward large-scale autonomous marine pollution monitoring," *IEEE Internet of Things Magazine*, vol. 4, no. 1, pp. 40–45, 2021.

[5] M. Sandra, L. I. Devriese, A. M. Booth, B. De Witte, G. Everaert, J. Gago, F. Galgani, K. Langedock, A. Lusher, T. Maes, H. Pirlet, J. Russell, and C. K. Pham, "A systematic review of state-of-the-art technologies for monitoring plastic seafloor litter," *Journal of Ocean Engineering and Science*, 2023. [Online]. Available: https://www.sciencedirect.com/science/article/pii/S2468013323000372

[6] G. Soldi, D. Gaglione, S. Raponi, N. Forti, E. d'Afflisio, P. Kowalski, L. M. Millefiori, D. Zissis, P. Braca, P. Willett, A. Maguer, S. Carniel, G. Sembenini, and C. Warner, "Monitoring of critical undersea infrastructures: The nord stream and other recent case studies," *IEEE Aerospace and Electronic Systems Magazine*, vol. 38, no. 10, pp. 4–24, 2023.

[7] X. Wang, X. Fan, P. Shi, J. Ni, and Z. Zhou, "An overview of key slam technologies for underwater scenes," *Remote Sensing*, vol. 15, no. 10, 2023. [Online]. Available: https://www.mdpi.com/2072-4292/15/10/2496

[8] M. Sung, J. Kim, H. Cho, M. Lee, and S.-C. Yu, "Underwater-sonar-image-based 3d point cloud reconstruction for high data utilization and object classification using a neural network," *Electronics*, vol. 9, no. 11, 2020. [Online]. Available: https://www.mdpi.com/2079-9292/9/11/1763

[9] C. Kun, X. Feng, and Y. Juan, "Three dimensional reconstruction of forward-looking sonar images based on oren and nayar model," in *2021 OES China Ocean Acoustics (COA)*, 2021, pp. 1011–1015.

[10] L. R. Fuchs, A. Gällström, and A. Maki, "Towards dense point correspondence with patchmatch in low-resolution sonar images," in *2022 IEEE/OES Autonomous Underwater Vehicles Symposium (AUV)*, 2022, pp. 1–6.

[11] M. Labbé and F. Michaud, "Rtab-map as an open-source lidar and visual simultaneous localization and mapping library for large-scale and long-term online operation," *Journal of Field Robotics*, vol. 36, no. 2, pp. 416–446, 2019. [Online]. Available: https://onlinelibrary.wiley.com/doi/abs/10.1002/rob.21831

[12] T. Foote, "tf: The transform library," in *Technologies for Practical Robot Applications (TePRA), 2013 IEEE International Conference on*, ser. Open-Source Software workshop, April 2013, pp. 1–6.

[13] G. Chen, J. Yang, B. Huang, C. Ma, F. Tian, L. Ge, L. Xia, and J. Li, "Toward digital twin of the ocean: from digitalization to cloning," *Intelligent Marine Technology and Systems*, vol. 1, no. 1, p. 3, 2023.